A.C. Conductivity and Electrical Modulus Studies of $Li_{1.3}Al_{0.3}Ti_{1.7}(PO_4)_3$ Electrolyte Thin Films Grown by RF Magnetron Sputtering

Kamatam Hari Prasad [a,b], Ratnakar Arumugam [a,c], E.S. Srinadhu [d], N. Satyanarayana [a, *]

[a]Department of Physics, Pondicherry University, Puducherry – 605014, India.
[b] Institute of Aeronautical Engineering, Dundigal, Hyderabad – 500 043, India.
[c] Centre for Nanoscience and Technology, Pondicherry University, Puducherry – 605014, India.
[d] LAM Research Corporation, Fremont, CA, 94538, USA
*Corresponding author: Tel: 0413-2654404; E-mail: nallanis2011@gmail.com

ABSTRACT

$Li_{1.3}Al_{0.3}Ti_{1.7}(PO_4)_3$ (LATP) electrolyte thin films were deposited on aluminum oxide (Al_2O_3) substrate at ambient temperature by RF magnetron sputtering method. The as-grown LATP thin film was post-annealed up to 500 ^oC in the presence of oxygen to enrich the crystallinity of the thin film. XRD results confirm the formation of the crystalline phase of the LATP thin film annealed at 500 ^oC. AFM micrographs of LATP thin films revealed the surface morphology and roughness properties. The ac conductivity, dielectric constant (ε′), and electric modulus (M′′) for the as-deposited and post-annealed LATP thin films were evaluated by analyzing measured impedance data as a function temperature in the frequency range of 100 Hz to 10 MHz.

Keywords: RF magnetron sputtering, $Li_{1.3}Al_{0.3}Ti_{1.7}(PO_4)_3$ electrolyte thin-film, XRD, impedance, AC conductivities, dielectric constant, electrical modulus.

1 INTRODUCTION

Lithium-ion batteries with high energy density, power density, and long charge-discharge cycle life, etc., are considered to be one of the most promising energy storage devices for portable electronic devices as well as electric vehicles applications [1-7]. Recently, all-solid-state thin film micro-batteries have drawn more attention due to many advantages such as corrosion free, leak proof, ruggedness, long self-life, long cycle life, thermal stability, miniaturization, light weight, specific capacity, high power density, etc., and also their potential applications as power sources for micro- and nano-devices such as smart cards, implantable medical devices, complementary metal oxide semiconductors (CMOS), liquid crystal displays (LCDs), memory chips, micro-electro-mechanical systems (MEMS) and nano-electro-mechanical systems (NEMS), etc. Also, the solvent-free all-solid-state rechargeable lithium-ion batteries are the most suitable, as per as safety is concerned, for their use in large-scale battery systems. For this, polymer and ceramic solid electrolytes have been developed and studied to eliminate the flammable components in the rechargeable Li-ion battery. Particularly, all-solid-state batteries with ceramics solid electrolyte are recognized as an ultimate safe battery.

Many deposition methods such as chemical vapor, spray pyrolysis, dip coating, radio-frequency magnetron sputtering (RFMS) and pulsed laser deposition techniques, etc., have been used for the fabrication of thin film electrodes [16-18]. Among them, RFMS deposition is the most versatile technique for the fabrication of thin films, which offers precise control over film thickness, higher sputter rates at lower Ar pressures and less deviation from the target stoichiometric composition.

Hence, in the present work, attempts were made to grow the nanocrystalline LATP electrolyte thin films on Al_2O_3 substrate at ambient temperature by RF magnetron sputtering. All the prepared thin films were annealed at 300 ^oC, 400 ^oC, and 500 ^oC under an oxygen atmosphere to enhance the crystallinity. All the as prepared as well as the annealed thin films were characterized using XRD, AFM and also studied their AC conductivity, dielectric constant and electric modulus properties by analyzing the measured impedance data using the win fit software.

2 EXPERIMENTAL TECHNIQUES

2.1 Preparation of LATP Electrolyte Thin Films

High purity (99.99%) spinel LATP target (50.88 mm diameter and thickness of 3 mm) bonded to the copper backing plate was purchased from Testbourne Pvt. Ltd., USA. As purchased LATP target was fixed to the magnetron and the distance between Si substrate and LATP target was fixed at 15 cm. A turbomolecular and rotary, as the backup, pumps were used to obtain the chamber base pressure of 1×10^{-7} Torr and then passed ultra-high pure Ar gas into the chamber through mass flow controller. The pre-sputtering process was performed for about 15 min. to remove surface contamination on LATP target and on Al substrate. Prior to the deposition of LATP material, a thin titanium (Ti) film of ~ 25 nm was sputtered onto Si substrate to serve as an adhesive layer. LATP thin films

were deposited on Al_2O_3 substrate by using RFMS power of 100 W at room temperature under an argon atmosphere at 1×10^{-3} Torr pressure. The thickness of the deposited LATP thin films was measured using a quartz crystal thickness monitor. The as-deposited LATP films were annealed at different temperatures 300, 400 and 500 ^oC in a pure oxygen atmosphere. Table 1 represents the sputtering deposition conditions for the spinel LATP thin films deposited on the Al_2O_3 substrate by using RFMS technique.

2.2 Characterization

XRD patterns of LATP films were recorded using the PANalytical, Philips, X' Pert Pro X-ray diffractometer having monochromatic X-ray source of CuK_α radiation with a wavelength (λ) of 1·541060 Å, operated at 40 kV and 30mA. Atomic Force Microscopy (AFM) images of the LATP films were recorded using the NanoScope-V Multimode^{TM} SPM, Veeco Instruments. The impedance measurements were made on LATP thin films of the as-deposited and post-annealed at different temperatures in the frequency range from 100 Hz to 10 MHz using Alpha A high-performance frequency analyzer of Novocontrol, Germany. The measured impedance data and the dimensions of LATP thin films were used for calculating AC conductivity (σ_{ac}), dielectric permittivity (ε') and electric modulus (M") of LATP thin films.

3. RESULTS AND DISCUSSION

3.1 XRD

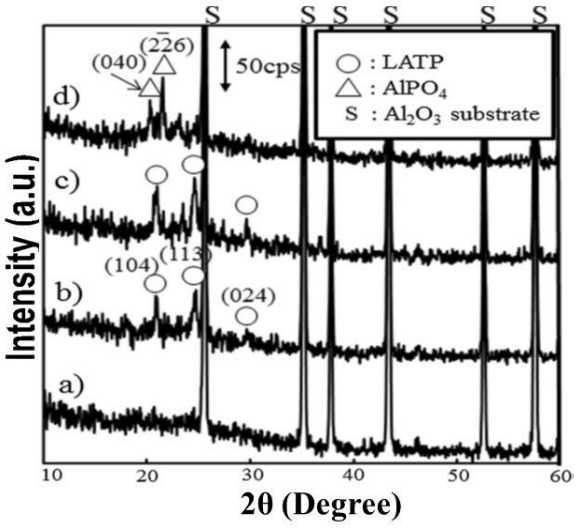

Fig.1 X-ray diffraction patterns of LATP thin films (a) as-deposited, (b) 300 ^oC, (c) 400 ^oC, and (d) 500 ^oC.

Fig.1 shows the XRD patterns of as-deposited and post-annealed at 300, 400 and 500 ^oC LATP thin films grown by RF magnetron sputtering on Al_2O_3 substrate. From fig. 1 (a), it is observed that as-deposited film exhibited peaks free XRD pattern, which confirm the formation of the amorphous phase of LATP thin film. The observed XRD peaks, marked as S is due to the pristine phase of substrate peak. From fig. 1 (b, c, and d), it is observed that the intensity of the XRD peaks increase with the increase of substrate temperature. From fig. 1(d), the observed XRD peaks of the LATP thin film post-annealed at 500 ^oC are in good agreement with the LATP (ICDD 00–035–0754) data and also good agreement with those reported in the literature.

3.2 AFM Micrographs

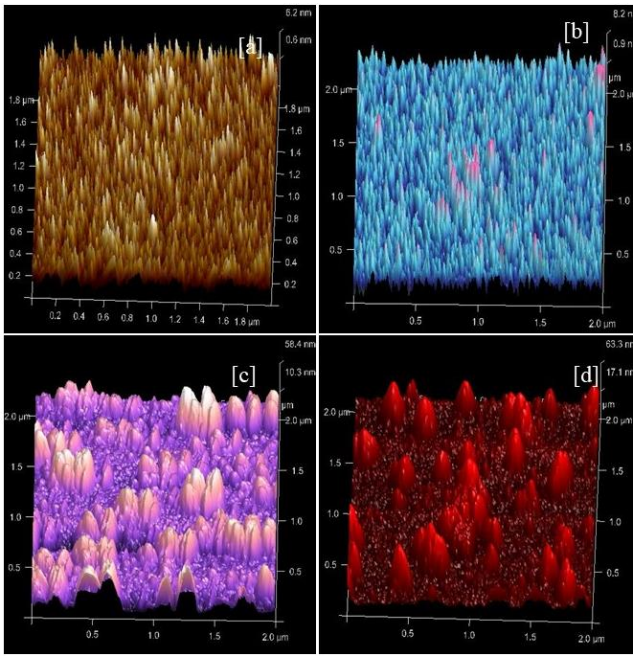

Fig. 2. 3D AFM micrographs of the LATP thin films of [a] as-deposited, and post-annealed at [b] 300 ^oC, [c] 400 ^oC, and [d] 500 ^oC.

From fig. 2 (a, b, c, d), AFM images clearly show that the grain size increases with post-annealing temperatures. From fig. 2 a, 3D AFM images of the as-deposited LATP thin film shows smaller individual grains with lower roughness. From fig. 2 (b, c, and d), it is observed that 3D AFM images of LATP thin films post-annealed at 200, 300, 400 and 500 ^oC show the denser granular structure and dense morphology is observed particularly for the post-annealed LATP thin film at 500 ^oC.

3.3 AC Conductivity (σ_{ac})

Fig. 3. Shows the Log (σ) vs. Log (ω) plots obtained at room temperature of LATP thin films of as-deposited and post-annealed at different temperatures (200 ^oC, 300 ^oC, 400 ^oC, and 500 ^oC). From fig.3, the frequency dependent conductivity plots showed two distinct regions within the measured frequency window, (i) the low-frequency plateau

region and (ii) high-frequency dispersion region. The plateau region corresponds to frequency independent conductivity $\sigma_{(0)}$ or dc conductivity (σ_{dc}) and it is evaluated by extrapolating the plateau region to the zero frequency (Y-axis). The frequency independent conductivity may be attributed to the long-range transport of free charge carriers with the applied field in LATP thin films. The observed a.c. conductivity in the high-frequency dispersion region follows Jonscher's universal power law (JUPL).

$$\sigma_{(\omega)} = \sigma_{(0)} + A\omega^{s} \quad (1)$$

where $\sigma_{(\omega)}$ is the ac conductivity, $\sigma_{(0)}$ is the zero frequency limit of $\sigma_{(\omega)}$, A is a constant, and *s* is the power law exponent ($0 < s < 1$). From fig. 3, it is also observed that the frequency at which the dispersion region deviated from the plateau is defined as the hopping frequency (ω_p), where, the initiation relaxation effects. An increase of a.c. conductivity with the increase of annealing temperature at the high frequency in LATP thin films is due to hopping of electrons between adjacent sites, results in local displacement of charges in the direction of the applied frequency [7-16].

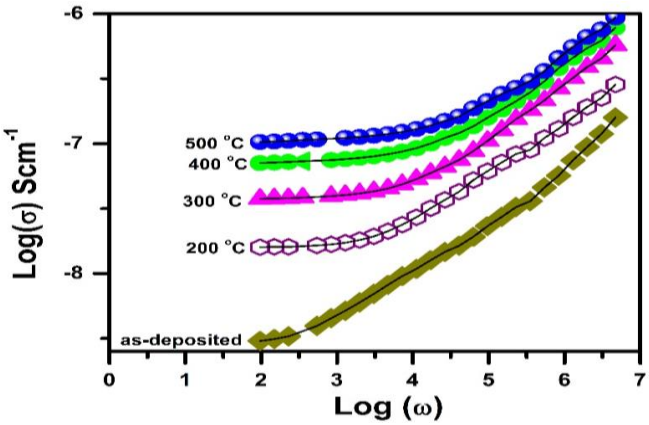

Fig. 3. Log (σ) vs. Log (ω) plots obtained at room temperature of LATP thin films of as-deposited and post-annealed at different temperatures (200 °C, 300 °C, 400 °C, and 500 °C).

3.4 Dielectric constant (ε')

From fig. 4, it is observed that, with the increase of frequency, dielectric permittivity (ε') decreases and attains a constant value at high frequencies and it is also observed that the dielectric permittivity increases with the increase of temperature. From fig.4, the observed dielectric permittivity (ε') at high frequencies may attribute to the periodic reversal of the high electric field results in no charge accumulation at the interface and hence, the dielectric permittivity (ε') remain constant. The motion of the charge without accumulation can be explained in terms of the carrier's diffusion mechanism. From fig. 4, the increase of dielectric permittivity (ε') with the decrease in frequency can be attributed to the contribution of charge accumulation at the interface, which results in the formation of space charge region at the electrode and electrolyte interface. This will hinder the motion of the mobile charge carriers in the sample and hence, the dielectric permittivity (ε') value increases with the decrease of frequency. From fig. 4, the increase of dielectric permittivity (ε') with increasing temperature may be due to the increase of thermal activation and local displacement of charge carriers, which may help to increase the dielectric permittivity (ε') with the increase of temperature [7-16].

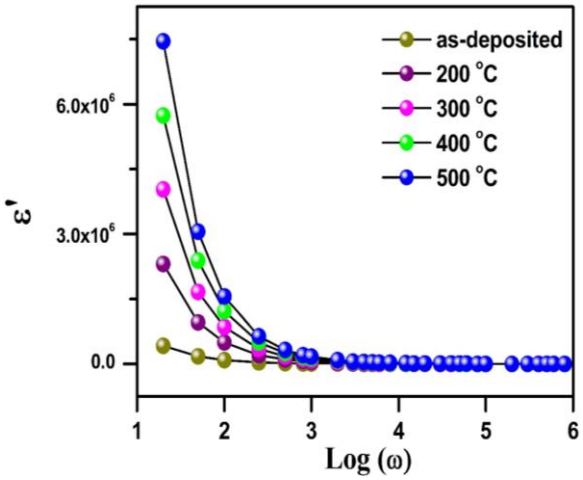

Fig. 4. The real part of dielectric constant (ε') versus frequency plots obtained at room temperature of LATP thin films of as-deposited and post-annealed at different temperatures (200 °C, 300 °C, 400 °C, and 500 °C).

3.5. Electrical Modulus

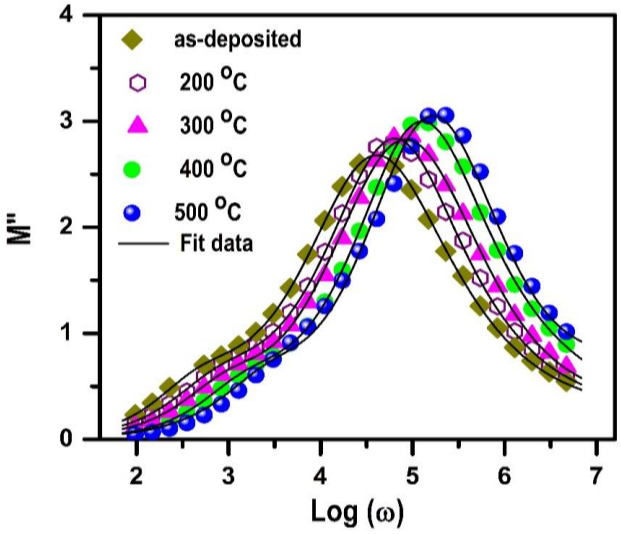

Fig. 5. The imaginary part of the electric modulus (M'') versus Log (ω) obtained at room temperature of LATP thin films of as-deposited and post-annealed at various temperatures (200 °C, 300 °C, 400 °C, and 500 °C).

Fig. 5. Shows the imaginary part of the electric modulus (M") versus Log (ω) obtained at room temperature of LATP thin films of as-deposited and post-annealed at various temperatures (200 ^{o}C, 300 ^{o}C, 400 ^{o}C, and 500 ^{o}C). From fig. 5, it is observed that the peak exhibit at the relaxation frequency (f_{max}) and the position of the peak frequency shifting towards higher frequency regions and also the broadness of electric modulus (M") curve increases with the increase of annealing temperature. However, the shift of the peak position appears to move towards higher frequency region with the increasing annealing temperatures of the samples and this can be attributed to the variation of relaxation processes of the mobile charge carriers following the non-Debye type behavior in LATP thin films [7-16].

4 CONCLUSION

Spinel LATP electrolyte thin films were successfully deposited on Ti/Al_2O_3 substrate at ambient temperature by RF magnetron sputtering technique. The crystalline phase of LATP electrolyte thin film was obtained at lower annealing temperature at 500 ^{o}C. The phase purity of the LATP electrolyte thin films was confirmed by XRD results. The AFM results were confirmed by the spherical morphology, crystalline phase and denser granular structure with the less surface roughness of LATP thin films. The evaluated AC conductivity (σ_{ac}) and dielectric constant (ε') values are found to increase with the rise in the annealing temperatures of LATP thin films. The imaginary part of the electric modulus (M") studies revealed the non-Debye nature of LATP thin films.

ACKNOWLEDGMENT

NS would like to thank the DST-Nano mission, Govt. of India, for providing grants in the form of research project sanction letter No.: SR/S5/NS-49/2005, dated on 30-07-2010 and NRB-DRDO, Govt. of India, for providing grants in the form of research project sanction letter No.: NRB-377/MAT/16-17, dated on 19-04-2016, respectively for developing five targets DC/RF magnetron sputtering system and electrochemical system facilities for developing and characterizing all-solid-state thin film lithium-ion micro-batteries.

REFERENCES

[1] K. Dokko, K. Hoshina, H. Nakano, K. Kanamura, J. Power Sources 174 (2007) 1100–1103.
[2] S.S. Das, P.K. Srivastava, N.B. Singh, J. Non-Cryst. Solids 358 (2012) 2841–2846.
[3] P. Knauth, Solid State Ionics 180 (2009) 911–916.
[4] A. Chandra, A. Bhatt, A. Chandra, J. Mater. Sci. Technol. 29 (2013) 193–208.
[5] J.F.M. Oudenhoven, L. Baggetto, P.H.L. Notten, Adv. Energy Mater. 1 (2011) 10–33.
[6] A. Ratnakar, K. Hari Prasad, S. Vivekananthan, P C Karthika, Aashutosh Kumar, Material Today: Proceedings, 3(10) (2016) 4052-4057.
[7] Kamatam Hari Prasad, S. Vintoth, P. Jena, M. Venkateswarlu, N. Satyanarayana, Materials Chemistry and Physics, **194** (2017) 188-197.
[8] Kamatam Hari Prasad, S. Subramanayam, T.N. Sai ram, G. Amarendra, E.S. Srinadh, N. Satyanarayana, Journal of Alloys and Compounds, **718** (2017) 459-470.
[9] K. Hari Prasad, A. Ratnakar, Aashutosh Kumar, N. Satyanarayana, Material Today: Proceedings, **3(10)** (2016) 4064-4069.
[10] Paramananda Jena, N. Nallamuthu, K. Hariprasad, M. Venkateswarlu, N. Satyanarayana, Journal of Sol-gel Science and Technology, **72** (2014) 480-489.
[11] K. Hari Prasad, N. Naresh, B. Nageswar Rao, M. Venkateswarlu, N. Satyanarayana, Material Today: Proceedings, **3(10)** (2016) 4040-4045.
[12] K. Hari Prasad, P. Muralidharan, E.S. Srinadhu, N. Satyanarayana, Advanced Materials - TechConnect Briefs 2017, 2 (2017) 106-109.
[13] K. Hari Prasad, P. Muralidharan, E.S. Srinadhu, N. Satyanarayana, Advanced Materials - TechConnect Briefs 2017, 2 (2017) 90-93.
[14] K. Hari Prasad, P. Muralidharan, E.S. Srinadhu, N. Satyanarayana, Advanced Materials - TechConnect Briefs 2017, 2 (2017) 114-117.
[15] K. Hari Prasad, S. Vinoth, A. Ratnakar, N. Satyanarayana, Material Today: Proceedings, **3(10)** (2016) 4046-4051.
[16] P. Muralidharan, N. Nallamuthu, I. Prakash, N. Satyanarayana, J. Am. Ceram. Soc., 90 (2007) 125-131.